THE JOURNAL OF PHYSICAL CHEMISTRY C
A JOURNAL OF THE AMERICAN CHEMICAL SOCIETY

pubs.acs.org/JPCC
Article

Methanol-Mediated Hydrogen Transfer Reactions at Surface Lewis Acid Sites of H-SSZ-13

Annika E. Enss, Philipp Huber, Philipp N. Plessow,* and Felix Studt*

Cite This: https://doi.org/10.1021/acs.jpcc.4c03408
Read Online

ACCESS | Metrics & More | Article Recommendations | Supporting Information

ABSTRACT: Lewis acid sites (LAS) at the CHA(001) and CHA(101) surfaces are investigated regarding their activity for MeOH-mediated hydrogen transfer reactions from MeOH to alkenes, yielding alkanes and formaldehyde. Direct MeOH decomposition to formaldehyde and hydrogen is also investigated. Furthermore, the coupling of the produced olefins with formaldehyde to dienes and H_2O via the Prins reaction is studied. The reactivity of LAS for these reactions is compared to that of bulk Brønsted acid sites (BAS) and surface BAS. Periodic density functional theory (DFT) is used in connection with DLPNO-CCSD(T) calculations on cluster models. Hydrogen transfer reactions are found to be often more favorable on LAS, while both LAS and BAS have similar activity for Prins reactions.

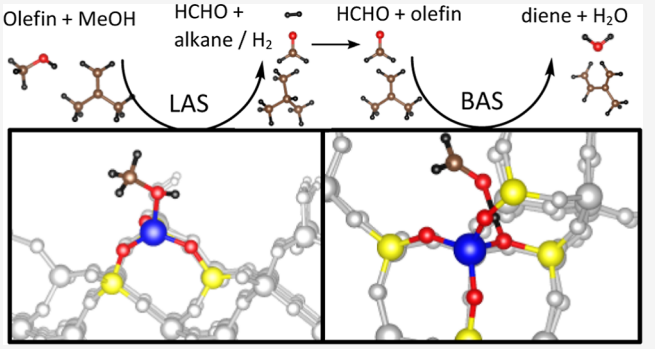

INTRODUCTION

In the transformation of industrial chemical processes relying on fossil resources into sustainable and renewable processes, zeolite catalysts play an important role to making the utilization of renewable resources possible. The methanol-to-olefins (MTO) process produces hydrocarbons from methanol, which can be synthesized from syngas (H_2 + CO) and thus potentially also biomass or green hydrogen.[1−6] The reaction network of the MTO process is complex and involves two different reaction cycles using aromatics or olefins as cocatalysts, the so-called hydrocarbon pool (HCP).[7−9] Olefin and aromatic cycles both produce olefins and are interconnected by hydrogen transfer (HT) reactions between alkenes, producing alkanes and dienes. Catalyst deactivation through coking is one of the main challenges in the MTO process. Rather than a well-defined chemical substance, coke refers to all kinds of immobile (large) hydrocarbons that clog the pores of zeolites, thus hindering the diffusion of reactants and products and also restricting access to active sites.[1,10,11] Bulky aromatic species, for example, condensated aromatics such as naphthalene, are believed to be a major contributor to coke.[12−15] Dienes are the main precursor for aromatics (and eventually coke), and they are expected to form through HT reactions between olefins that are disproportionate to alkanes and dienes.[16−19] Formaldehyde is recognized as an important intermediate in HTs that facilitates the formation of coke.[16,20−22] Among the strategies to reduce coke formation, both H_2O-[23] and H_2-cofeeding,[24−27] were investigated as ways to reduce effect of formaldehyde.

In 2016, Müller et al. observed that in the presence of MeOH, the formation of alkanes was much faster than after complete conversion of MeOH, so they proposed an alternative HT pathway from MeOH to alkenes, producing formaldehyde and alkanes[28] (Scheme 1, reaction 1a). The produced formaldehyde can couple with a second alkene in a Prins reaction, and the alcohol that is formed can dehydrate directly, generating dienes (Scheme 1, reaction 2). Liu et al. found that this reaction, rather than HT between two olefins forming alkanes and dienes, was the dominant pathway to produce dienes and finally aromatics.[29] Looking beyond zeolite catalysis, the methanol-mediated HT also shows similarities to further metal-catalyzed transfer hydrogenations.[30,31]

According to Müller et al., the Prins reaction takes place only at Brønsted acid sites (BAS), while the HT step between MeOH and alkenes is catalyzed by Lewis acid sites (LAS). In the MeOH-mediated HT pathway, formaldehyde is a crucial intermediate. Apart from MeOH-mediated HT, it can be formed by two alternative reactions. One is the direct decomposition of MeOH into HCHO and H_2 (Scheme 1, reaction 1b) as found in the absence of BAS,[32,33] and by HT of MeOH to a surface methoxy species (SMS) to form methane, formaldehyde, and water.[34,35] Wen et al. found the alternative production routes to HCHO to be more likely since they observed that HCHO formation rates were independent of

Received: May 23, 2024
Revised: August 6, 2024
Accepted: August 6, 2024

Scheme 1. Reactions Investigated in This Work: HCHO Formation by Hydrogen Transfer (HT) from MeOH to Alkenes for the Example of Isobutene (1a) and by Direct Decomposition of MeOH (1b)[a]

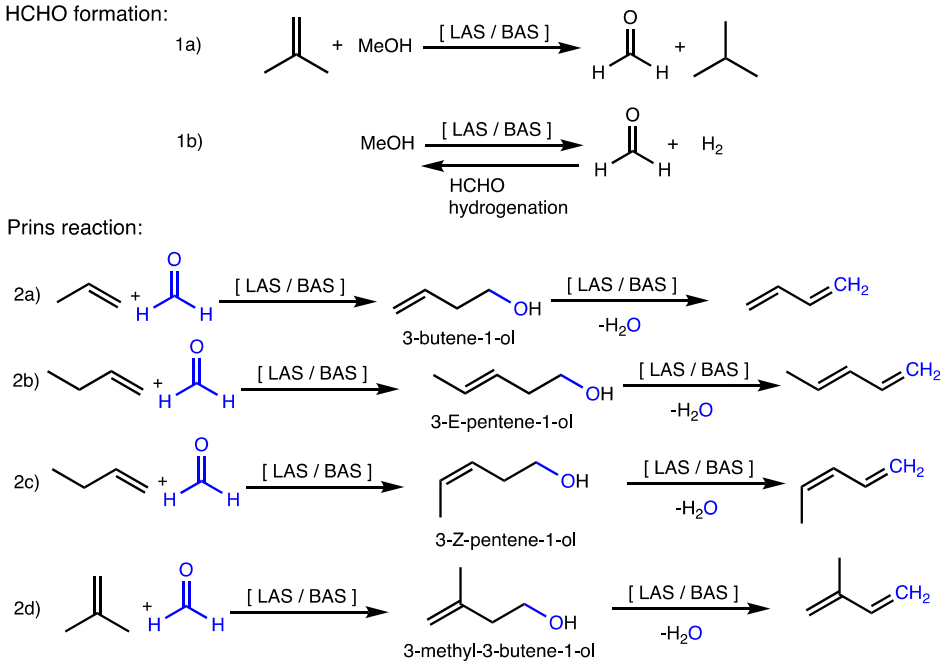

[a](2a–d): Prins reaction of HCHO and alkene to diene and H_2O.

olefin formation rates.[36] The study of Müller et al. uses H-ZSM-5 as a catalyst, suggesting that extraframework aluminum (EFAL) represents the largest part of LAS. While there is an increasing effort to determine the structure and reactivity of EFAL[37−39] and the framework-associated Al,[40,41] these are not the only possible LAS in zeolites. In recent studies, LAS on the outer surfaces of zeolite crystals have gained more attention.[42,43] Substitution of a silicon atom from a silanol group at the surface with an aluminum and a hydrogen atom for charge balance leads to water adsorbed on a tetrahedrally coordinated aluminum. After dehydration, a 3-fold coordinated Al remains that can act as LAS. Chizallet and co-workers investigated the surfaces of H-ZSM-5[42] and FAU zeolites[43] computationally regarding the stability and acidity of LAS and BAS motifs. The reactivity of LAS on CHA surfaces was investigated by Huber et al. for methanol dehydration to DME, which is the initial step in the MTO reaction network.[44] In that study, surface BAS was found to be similar in reactivity to bulk BAS,[44] and similar conclusions were reached by Hibbitts and co-workers for H-ZSM-5.[45]

In this work, the MeOH-mediated HT mechanism, diene formation, and MeOH decomposition are investigated on the surface LAS and BAS of CHA zeolite and with different reacting alkenes. The results are compared with the reactivity of BAS in the bulk zeolite. While this work focuses on surface LAS, other LAS, like EFAL sites, might differ in their reactivity and will be subject to future work.

COMPUTATIONAL DETAILS

Periodic DFT with the dispersion-corrected PBE-D3[46,47] functional and a convergence criterion of 0.001 eV/Å was applied to perform structure optimizations. Calculations were carried out with the Vienna Ab Initio Simulation Package[48] (VASP) version 5.4.1 using the atomic simulation environment[49] (ASE) with the projector-augmented wave method (PAW), an energy cutoff of 400 eV, and *k*-point sampling only at the Γ-point. Vibrational analysis was performed by calculating a partial Hessian of the adsorbate atoms and the acid site, consisting of the aluminum atom and all adjacent oxygen and silicon atoms (four each in the case of BAS and three in the case of LAS), with vibration displacements of 0.01 Å as the default of ASE. Gibbs free energies were calculated using the harmonic-oscillator approximation for adsorbed species, additionally applying rigid-rotator and free-translator approximations for gas species. Frequencies with a value lower than 12 cm^{-1} were raised to that value to prevent large entropic inaccuracies due to the harmonic-oscillator approximation.[50,51] The MTO process is typically carried out at reaction temperatures of 350−450 °C,[1] we therefore chose 400 °C for Gibbs free energies to model reaction temperature. Transition states were calculated with automated relaxed potential energy surface scans[52] (ARPESS). To confirm the connectivity of transition states, structures were distorted along the direction of the transition mode and subsequently optimized toward the end points. When the structures of single adsorbed molecules were optimized, several orientations of the molecules were probed in order to find the most stable structure. Geometries of coadsorbed molecules were determined as end-points of geometry optimization after distortion of transition states. To alleviate the limitations of approximate DFT, Sauer and co-workers established the use of cluster models for the active site, which allow to employ higher-level methods.[53−56] We employ the following correction scheme[57]

$$\Delta E^{\text{cluster}} = \Delta E^{\text{cluster}}_{\text{MP2/CBS}} + E^{\text{cluster}}_{\text{DLPNO-CCSD(T)/DZ}} - E^{\text{cluster}}_{\text{PBE-D3}} \quad (1)$$

This energy correction term is added to the periodic DFT energy and contains the PBE-D3 energy of the cluster model ($E^{\text{cluster}}_{\text{PBE-D3}}$), the DLPNO-CCSD(T) energy ($E^{\text{cluster}}_{\text{DLPNO-CCSD(T)/DZ}}$), and the difference between MP2/CBS (complete basis set)

https://doi.org/10.1021/acs.jpcc.4c03408
J. Phys. Chem. C XXXX, XXX, XXX−XXX

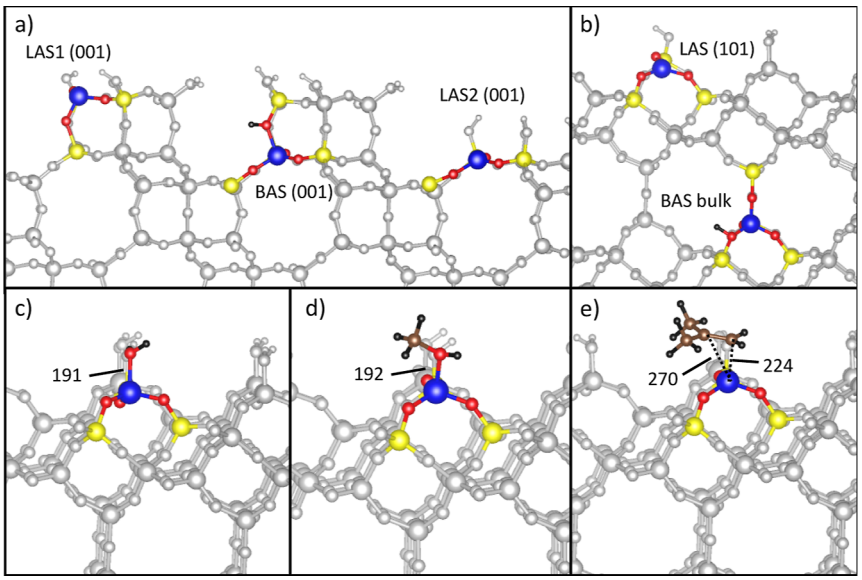

Figure 1. Investigated Lewis and Brønsted acid sites on (a) the (001) surface and (b) the (101) surface and in the bulk zeolite. Adsorption of (c) H_2O, (d) MeOH, and (e) isobutene on LAS (101). Bond distances are indicated in pm. Color code: blue: aluminum, yellow: silicon, red: oxygen, brown: carbon, and black: hydrogen.

extrapolation and MP2/ccpVDZ calculations ($\Delta E^{\text{cluster}}_{\text{MP2/CBS}}$). This term includes HF energy and MP2 correlation separately extrapolated with cc-pVDZ, cc-pVTZ, and cc-pVQZ basis sets using three-point exponential fit[58] and cc-pVDZ and cc-pVTZ using the two-point X^{-3} fit,[59] respectively. For HF, MP2, and CCSD(T) calculations, the ORCA program package (version 4.2.1) was used.[60] The basis sets used were cc-pVDZ and cc-pVXZ[61] with X = D,T for CCSD(T) and MP2, respectively. The "TightPNO" threshold was used in the DLPNO approximation.[62−64] Basis sets cc-pVXZ with X = D,T,Q and the RIJCOSX approximation[65] with GridX6 were used for HF calculations. Nonperiodic DFT calculations were carried out with the TURBOMOLE V7.4.1 program package,[66] using the PBE-D3 functional, def2-TZVPP basis set,[67,68] and the resolution of the identity approximation.[69]

Cluster models of BAS(001), LAS1(001), LAS2(001), LAS(101), and bulk BAS contain 52, 52, 39, 64, and 46 T-sites, respectively.

RESULTS AND DISCUSSION

Investigated Sites. The H-SSZ-13 zeolite was used in this study as a model catalyst. It crystallizes in the chabazite (CHA) structure, where the lattice constants of 13.625, 13.625, and 15.067 Å were optimized in earlier studies.[70] The bulk structure contains one unique T-site and has a Si/Al ratio of 35:1. Surface structures were taken from earlier work.[44] Huber et al. investigated the stability and reactivity of several surface BAS and LAS of H-SSZ-13. First, they analyzed the stability of different surface facets, namely, the (101), (110), (001), and (100) surfaces. The most stable surface is the (101) surface, which has one possible LAS and two different BAS. In addition to the (101) surface, they also considered the (001) facet, which has been investigated in previous studies.[71] On this surface, two LAS and two BAS are possible. In this work, all three LAS on these two surfaces are considered, labeled LAS1(001), LAS2(001), and LAS(101). The unit cell of the (001) surface sites contains 36 T atoms with a slab thickness of approximately 15.0 Å, whereas the (101) surface has a unit cell containing 72 T atoms and a slab thickness of approximately 18.6 Å. The reaction barriers for BAS on both facets for DME formation are similar,[44] so we investigated only one BAS on the (001) facet [BAS (001)]. Finally, all reactions were also investigated at the bulk BAS. The investigated sites are depicted in Figure 1. The LAS is shown here in its three-coordinated form. When the model surface is constructed, a silanol group is replaced by an aluminum and one water molecule for charge balance. This H_2O is adsorbed strongly, but can desorb and be replaced by MeOH, while the clean LAS is 3-fold coordinated. Note that adsorbate exchange by adsorption/desorption via a 5-fold coordinate Al is less favorable than desorption/adsorption via a 3-fold coordinated Al (see Figure S4). Regarding the formation of the clean acid sites, we show in Figure S3 the intrinsic stabilities of the three LAS compared to their hydrated states, and we find that all three LAS can be formed from their hydrated states in the relevant temperature range of 500−650 °C. For BAS, both on the surface and in the bulk, transition states and adsorption energies were calculated with the acidic proton located at all four oxygen atoms adjacent to the aluminum, and only the structures with the lowest free energy are presented here.

Adsorption Energies. First, the adsorption energies of relevant reactants in this work were computed. These are the investigated alkenes and dienes (ethene, propene, 1-butene, isobutene, and 1,3-butadiene), the alcohols resulting from the Prins reaction, and other reactants (MeOH, H_2O, and HCHO). All oxygen-containing species are adsorbed with their oxygen atoms, while alkenes are adsorbed at their double-bond. The adsorption of MeOH, H_2O, and isobutene at LAS(101) is shown in Figure 1c−e. The Al−O distances of oxygen-bound species adsorbed at LAS are in the range of 188−196 pm, and the corresponding H−O distances of the same species adsorbed at BAS are in the range of 131−151 pm. Ethene is adsorbed at the LAS with similar Al−C distances to both carbon atoms of the double bond (244−252 pm), whereas the higher substituted alkenes have a shorter Al−C distance to the lower substituted carbon atom (223−238 pm) and a longer distance to the higher substituted carbon atom (259−274 pm). If the olefins are adsorbed at BAS, the C−H

https://doi.org/10.1021/acs.jpcc.4c03408
J. Phys. Chem. C XXXX, XXX, XXX−XXX

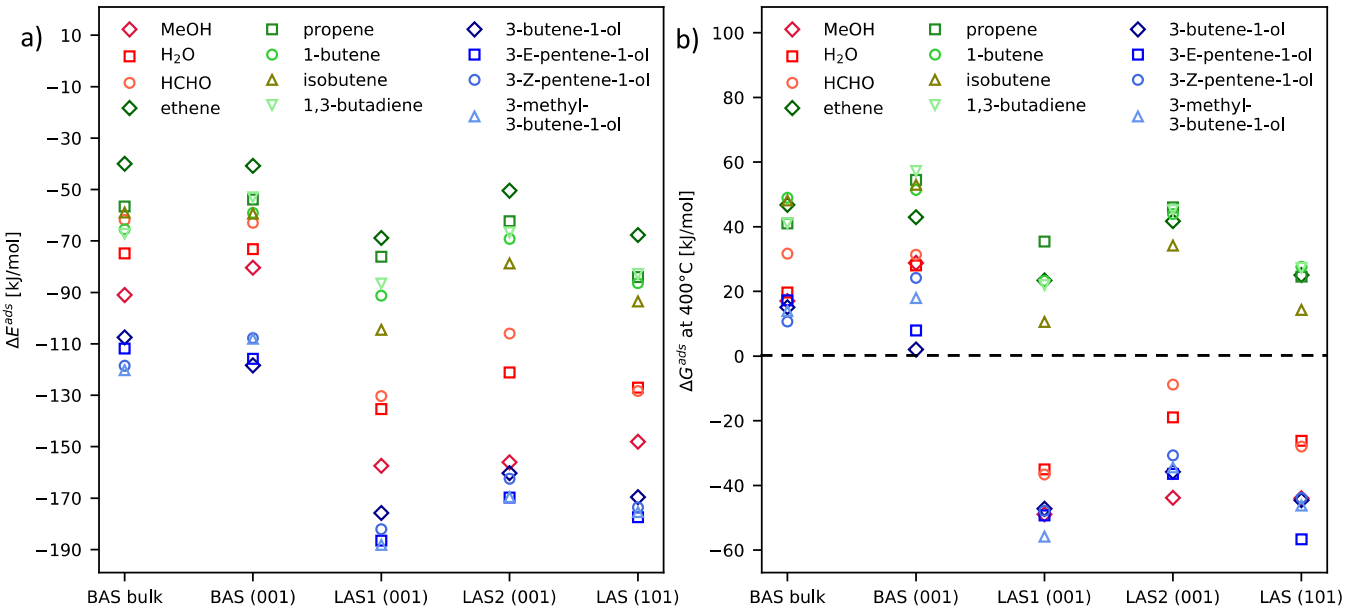

Figure 2. (a) Adsorption energies at all investigated acid sites and (b) adsorption free energies at 400 °C. Blue: intermediate alcohols of the Prins reaction, green: alkenes, and red: small oxygenates. Reference pressure: 1 bar.

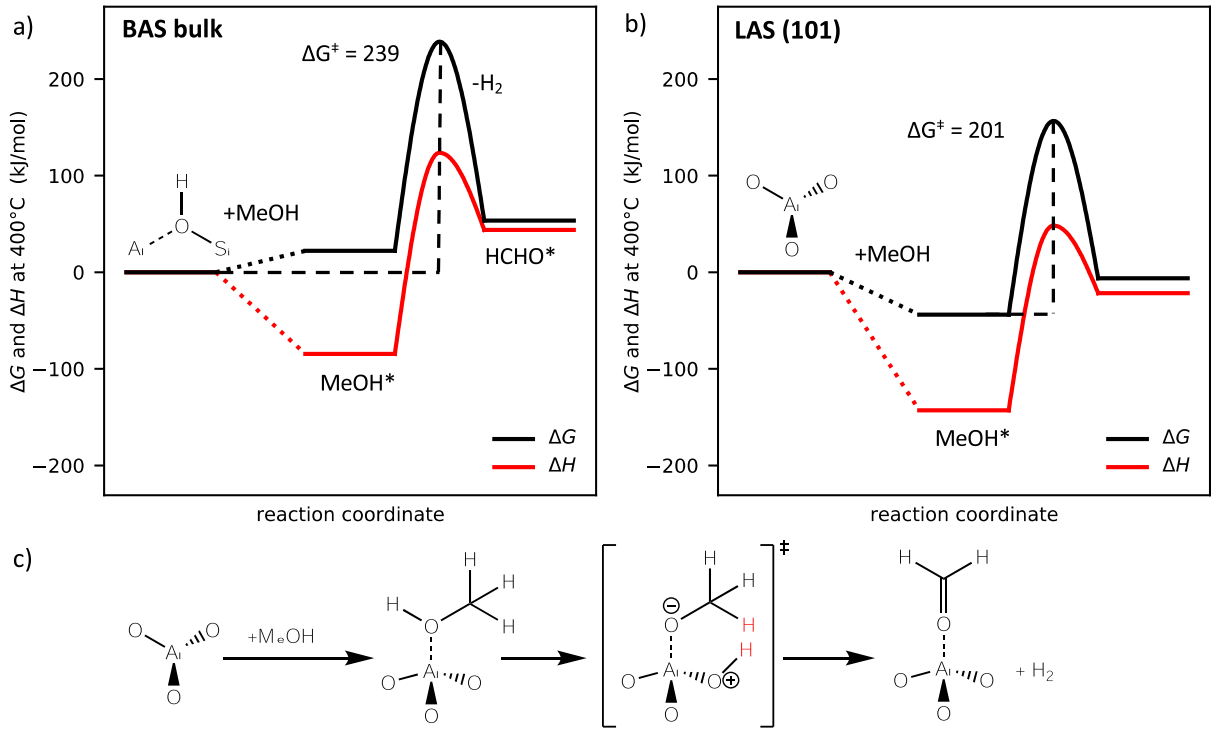

Figure 3. Comparison of free energies and enthalpies of the MeOH decomposition reaction at (a) bulk BAS and (b) LAS(101). (c) Reaction mechanism of MeOH decomposition at LAS. In the TS, both reacting hydrogen atoms are highlighted in red.

distances are in the range of 209−219 pm for ethene adsorption and in the ranges of 188−202 and 210−247 pm for the unsubstituted or substituted carbon atoms, respectively.

The calculated adsorption energies and free energies are shown in Figure 2. In general, alkenes have the lowest adsorption strength, so that in case of two coadsorbed species, the oxygen-containing molecule will be adsorbed directly at the acid site while the alkene is coadsorbed. At 0 K, the strongest adsorption energies are observed for the higher alcohols (blue), with a considerable gap compared to the group of smaller oxygenates (red). As can be seen on the right-hand side of Figure 2, the gap in adsorption free energies is smaller at 400 °C, with MeOH adsorption at LAS2(001) being stronger than adsorption of the higher alcohols. This is due to a higher entropic contribution to ΔG^{ads} for the higher alcohols (see Figure S1). Similarly, not only ethene has the highest values for ΔE^{ads} at all sites but also has the lowest entropic penalty at 400 °C and is therefore stronger adsorbed than other alkenes at 400 °C, the entropic contributions are shown in the Supporting Information. The symmetry number also has an

https://doi.org/10.1021/acs.jpcc.4c03408
J. Phys. Chem. C XXXX, XXX, XXX−XXX

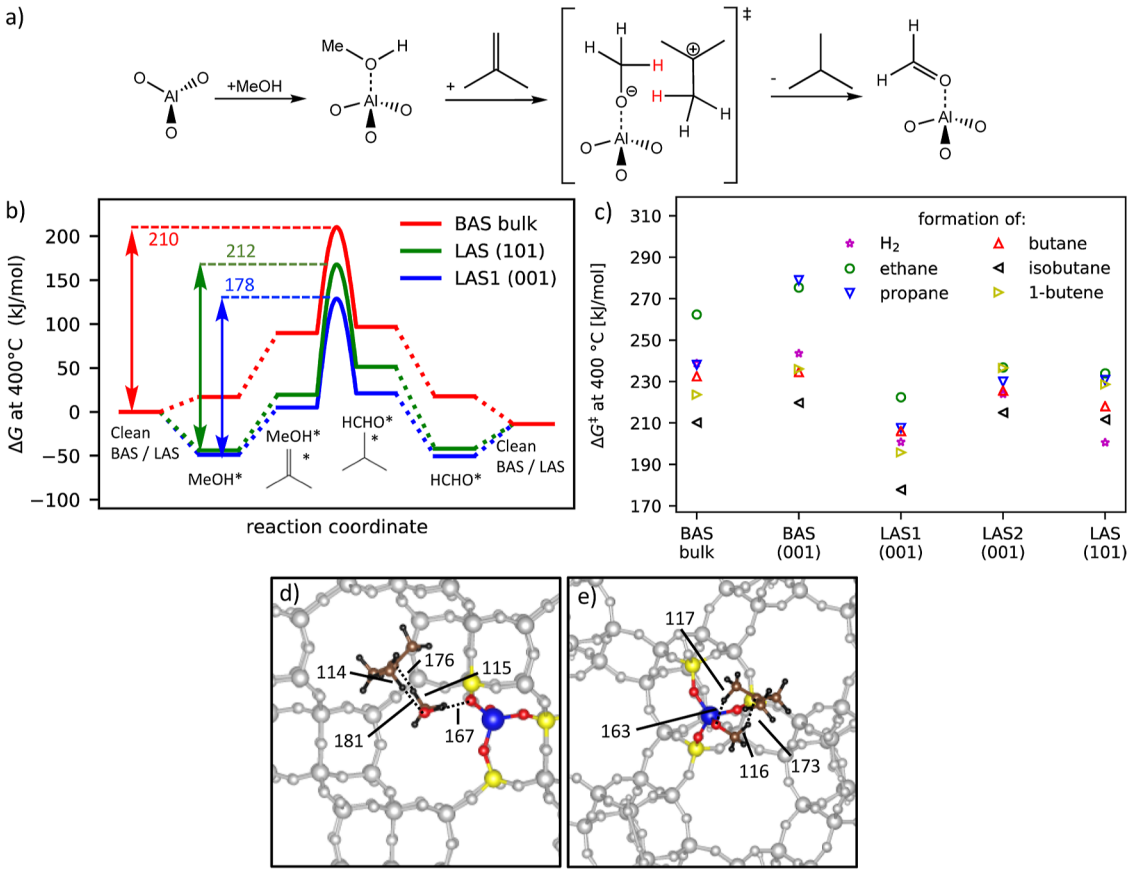

Figure 4. (a) Reaction mechanism scheme of the HT reaction with isobutene at LAS. In the TS, both reacting hydrogen atoms are highlighted in red. Indicated charges represent charge differences, for detailed Bader charge analysis of transition states, see Table S6. (b) Gibbs diagram of the HT reaction with isobutene at bulk BAS, LAS1(001), and LAS(101). Temperature is 400 °C and reference pressure is 1 bar for each reactant. References are the clean acid site and molecules in gas phase for BAS and MeOH adsorbed on the acid site with H-acceptor in gas phase for LAS. (c) Reaction barriers of HT with several olefins and MeOH decomposition at all investigated acid sites. Transition states of the HT reaction with isobutene at (d) bulk BAS and (e) LAS(101). Atomic distances are indicated in pm. Color code: blue: aluminum, yellow: silicon, red: oxygen, black: hydrogen, and brown: carbon.

influence on the calculated adsorption energies. With symmetry number 1, the adsorption of ethene would be weaker by 8 kJ/mol. The adsorption energies at both BAS are similar, while the adsorption energies at LAS are more dependent on the specific site. LAS2(001) has generally the highest adsorption energies, while the adsorption energies on LAS1(001) and LAS(101) are typically similar. Usually, all molecules adsorb stronger on LAS than on BAS. At the investigated reaction temperature of 400 °C, the adsorption free energy of the relevant reactants is still negative at LAS, while it is positive at BAS (see Figure 2b), making tetragonal Al sites with, e.g., adsorbed MeOH, the active LAS under the employed reaction conditions. Note also that the dissociation of MeOH on LAS is less favorable than MeOH adsorption.[44]

Reference State. According to the energetic span model,[72] the reference for transition state barriers is the preceding state having the lowest free energy. In our reactions, these are different states for BAS and LAS, respectively, which we show here to be exemplary for MeOH decomposition to HCHO and H_2, while the corresponding reaction barriers are discussed below. The free energies (ΔG) and enthalpies (ΔH) at 400 °C for this reaction are shown in Figure 3. The initial structure is the clean acid site and MeOH in the gas phase. The adsorption enthalpy of MeOH on BAS is negative, while the free energy is positive. At LAS, both the adsorption energy and the free energy are negative. These findings apply to all investigated reactions at BAS and LAS. Therefore, in all of the following calculations, the reference for the transition state energies is the clean acid site with the gas phase reactants for BAS. For LAS, however, the most stable reference state is always an adsorbed molecule such as MeOH. When two molecules react at the LAS, the reference state is usually the more strongly adsorbing molecule preadsorbed and the second molecule in the gas phase. Since DFT overestimates the strength of adsorption, we applied cluster model corrections at the CCSD(T)-level of theory as described in the Computational Details section. In Figure S2, the effect of this correction is shown for the adsorption free energies and transition state free energies. For adsorptions, this correction is generally lower than that for transition states.

Hydrogen Transfer. The HT between MeOH and alkenes, as proposed by Müller et al.,[28] was investigated for ethene, propene, 1-butene, isobutene, and 1,3-butadiene. The mechanism starts by the adsorption of MeOH and coadsorption of the alkene, and then both hydrogen atoms (Figure 4a), highlighted in red, are transferred in a single step to the double-bond of the alkene; we did not find a stable intermediate after the transfer of only one hydrogen atom. First, the double bond is protonated at the lower substituted carbon atom by the OH-group. The transition state consists of

https://doi.org/10.1021/acs.jpcc.4c03408
J. Phys. Chem. C XXXX, XXX, XXX−XXX

a carbocation and an alkoxide bound to the acid site, from which a hydride is transferred to the carbocation to form an alkane and formaldehyde. In Figure 4d,e, images of transition states are shown for the bulk BAS and LAS(101). Figure 4a shows the Gibbs free energy diagram of the HT reaction with isobutene for bulk BAS, LAS(101), and LAS1(001). In a zeolite crystal, bulk BAS is the BAS most abundantly present, and LAS(101) is expected to be the most abundant surface LAS. The LAS1(001) site is additionally shown because it leads to significantly lower reaction barriers than the other two LAS for all calculated reactions. Co-adsorption of two molecules is positive in free energy on both BAS and LAS. The Gibbs free energy diagram Figure 4a shows that the overall reaction barriers for isobutene at LAS(101) (212 kJ/mol) are slightly higher than in the bulk (210 kJ/mol), which is a difference within the accuracy of our calculations, but the barrier at LAS1(001) is smaller by about 30 kJ/mol (178 kJ/mol). The values of reaction barriers at the other sites and reactants are shown in Figure 4b. At 400 °C, reaction barriers for both BAS are >200 kJ/mol for all molecules, where the reaction with isobutene shows the lowest barriers [210 and 219 kJ/mol for bulk BAS and BAS(001), respectively].

The transition state of this reaction involves a carbocation, which is stabilized by a higher substitution of the carbon atom. Therefore, ethene has the highest reaction barrier due to the primary cation formed during the reaction. Propene, 1-butene, and 1,3-butadiene form secondary cations and have barriers more favorable than ethene. Isobutene is the only reactant that forms a tertiary cation, which explains why barriers are lower than for ethene by around 50 kJ/mol. At LAS, the differences between different acid site positions are more pronounced than for DME formation.[44] LAS1(001) is clearly favored over the second LAS at the same surface and also over LAS(101).

Methanol Decomposition and Formaldehyde Hydrogenation. An alternative to the HT from MeOH to olefins is the decomposition of MeOH to HCHO and H_2. It is a single-step reaction that includes two framework oxygens at BAS and one framework oxygen at LAS. The mechanism for LAS is shown in Figure 3c. First, one oxygen atom adjacent to aluminum is protonated by the OH-group of methanol, while the methoxy groups remain adsorbed at the aluminum atom. A H atom of the CH_3 group is then directly deprotonated to form HCHO and H_2. At BAS, methanol instead forms a hydrogen bond with its proton to an oxygen that does not carry the acidic proton. The CH_3 group is then protonated by the acidic proton, yielding again HCHO and H_2. The reaction at the BAS thus involves two oxygens (Figure 5b).

The reaction barriers are shown in Figure 4c. At 400 °C, the decomposition is more favorable on LAS [201, 223, and 201 kJ/mol for LAS1(001), LAS2(001), and LAS(101)] than on BAS [239 and 244 kJ/mol for bulk BAS and BAS(001)]. At LAS(101), which is the acid site on the thermodynamically most stable surface,[44] this barrier is 10 kJ/mol lower than the lowest HT barrier. The MeOH decomposition reaction on bulk BAS was also investigated in earlier work as part of the MTO initiation mechanism, where it competes with HT to a SMS, the latter leading to CH_4 instead of H_2 formation.[70]

The reverse reaction (hydrogenation of formaldehyde) is believed to be important in experiments with a H_2 cofeed,[24] and the reaction barrier we found here is lower than that of formaldehyde formation (Table 1). When cofeeding molecular hydrogen, catalyst lifetime increases, which can be explained by a suppression of dienes and aromatic formation via HCHO

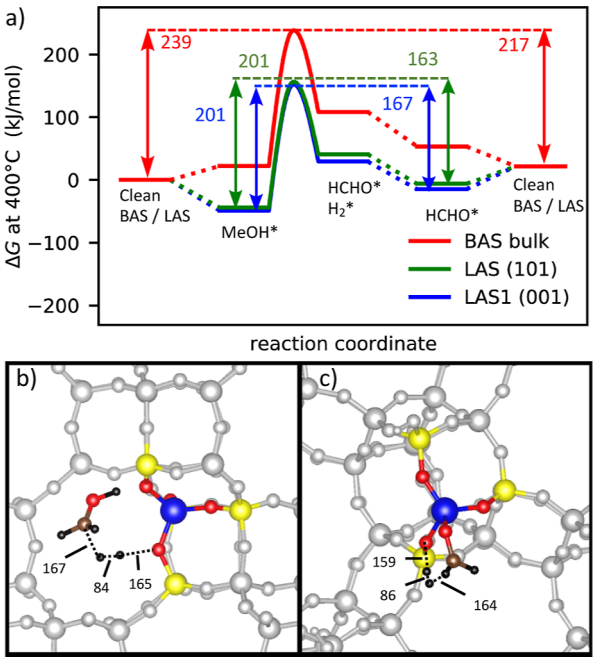

Figure 5. (a) Gibbs free energy diagram of MeOH decomposition at bulk BAS, LAS1(001), and LAS(101) at 400 °C and a reference pressure of 1 bar for each reactant. References are the clean acid site and MeOH/HCHO in the gas phase for BAS and MeOH/HCHO adsorbed on the acid site for LAS. Barrier heights are indicated in kJ/mol for the forward and backward reactions. Transition states of methanol decomposition at (b) bulk BAS and (c) LAS(101). Atomic distances are indicated in pm. Color code: blue: aluminum, yellow: silicon, red: oxygen, black: hydrogen, and brown: carbon.

hydrogenation.[24] In our calculations, hydrogenation barriers for HCHO are significantly lower at LAS (167, 167, and 163 kJ/mol) than at BAS (217 and 222 kJ/mol, see Table 1). But since MeOH adsorbs stronger than HCHO [by 12, 35, 16 kJ/mol at LAS1(001), LAS2(001), and LAS(101) and by 15 and 3 kJ/mol at BAS bulk and BAS(001)], surface LAS will likely be occupied by MeOH. This can also be seen in the Gibbs diagram in Figure 5a, where both reaction barriers for the forward and backward reactions are shown. When we do not consider our cluster model corrections, the PBE-D3 free energy barrier of HCHO hydrogenation at 350 °C is 142 kJ/mol and thus comparable to results in the literature for H-SSZ-13 (146 kJ/mol[26]). The cluster model corrections for surface sites are in the range of 38−55 kJ/mol for MeOH decomposition and in the range of 43−54 kJ/mol for HCHO hydrogenation.

Prins Reaction. In the Prins reaction, formaldehyde and an alkene couple first to a homoallylic alcohol, which is then dehydrated to the corresponding diene and H_2O. For this reaction, we found different reaction mechanisms for the two different acid site types (Scheme 2), whereas the mechanism is quite similar for the formaldehyde formation reactions.

The first reaction steps are identical for both LAS and BAS: the Prins coupling between formaldehyde and alkene occurs via a six-membered ring transition state structure, with the double bond between the second and third carbon atoms next to the alcohol group. This alcohol can now either dehydrate directly or be protonated by the BAS in a first step to dehydrate more easily. For LAS, protonation is not possible since it requires an acidic proton at the acid site. The reaction mechanism at LAS (Scheme 2a) shows therefore the direct

https://doi.org/10.1021/acs.jpcc.4c03408
J. Phys. Chem. C XXXX, XXX, XXX−XXX

Table 1. Reaction Free Energy Barriers for MeOH ⇄ HCHO + H_2 at 400 °C [kJ/mol][a]

reaction	bulk BAS	BAS(001)	LAS1(001)	LAS2(001)	LAS(101)
MeOH → HCHO + H_2	239	244	201	224	201
HCHO + H_2 → MeOH	217	222	167	167	163

[a]The initial and final states are taken to be the most stable ones in terms of Gibbs free energy, with MeOH and HCHO either adsorbed (LAS) or in the gas phase (BAS), which leads to different reaction free energies due to the difference in adsorption free energies for the LAS.

Scheme 2. (a) Reaction Scheme of the Prins Reaction with Propene and Butenol Dehydration at LAS; (b) Reaction Scheme of the Prins Reaction with Propene and Butenol Dehydration at BAS

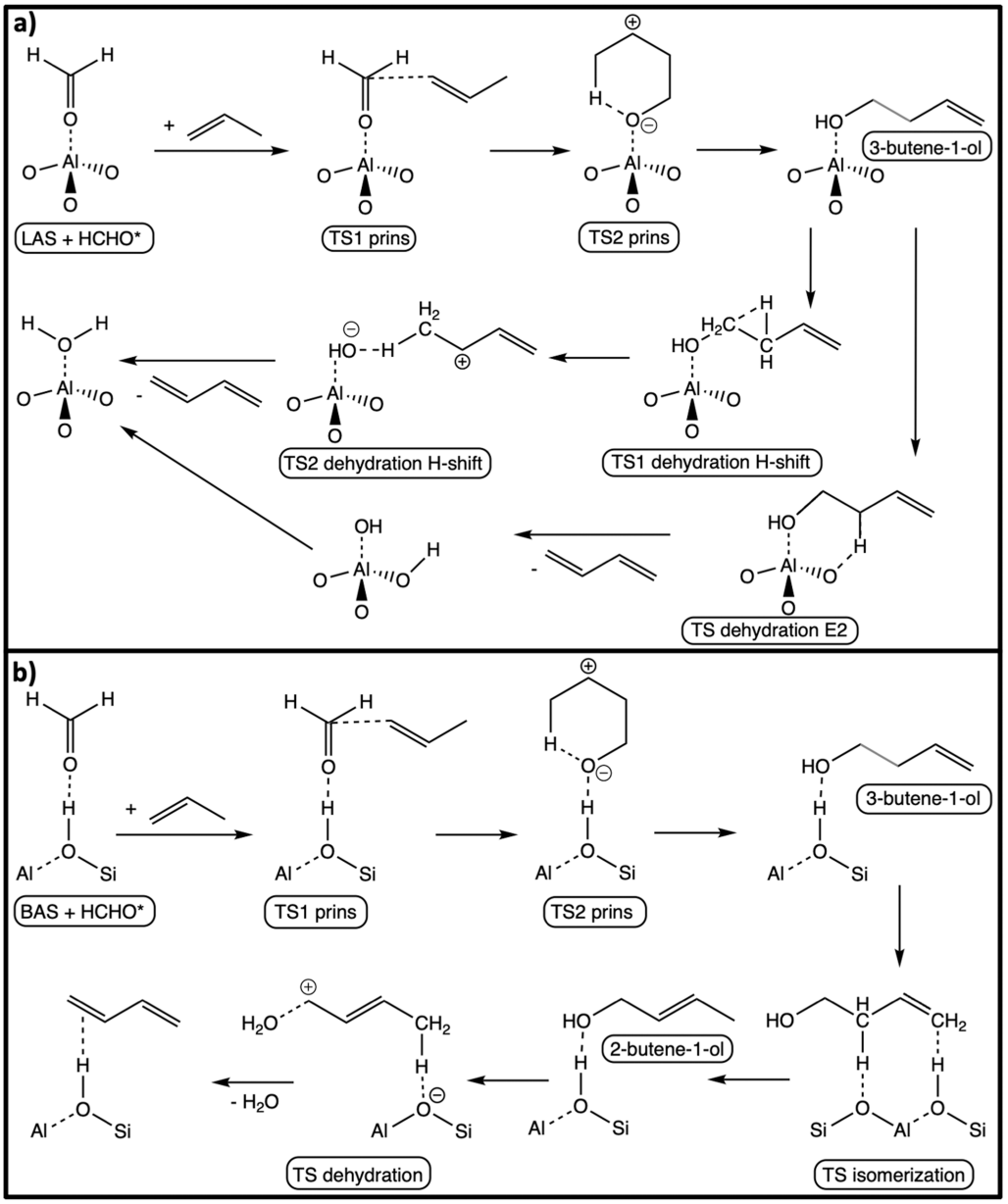

dehydration of the alcohol resulting from the Prins reaction, for which two different routes have been evaluated. In a process that can lead to either one concerted or two separate transition states, the C−O bond in the alcohol is broken first; this pathway is shown in the middle line of the reaction scheme. The resulting primary cation would be very unstable, and a hydrogen atom from the neighboring C atom immediately shifts to the terminal carbon, leading to a secondary cation (TS1 dehydration H-shift). In a second step, a proton from the terminal methyl group is abstracted by the OH-group bound to LAS, leading to diene and adsorbed H_2O (TS2 dehydration H-shift). In most cases, we found a transition state of one concerted reaction including these two dehydration steps, but for the sake of clarity, they are shown separately in the reaction scheme. A different pathway includes an E2-like dehydration mechanism similar to investigations by Larmier et al. for the dehydration of isopropanol,[73,74] shown in the third line of Scheme 2a. Here the C−O bond and the C−H bond at the neighboring carbon are broken simultaneously (TS dehydration E2), leading to the adsorption of an OH group on

https://doi.org/10.1021/acs.jpcc.4c03408
J. Phys. Chem. C XXXX, XXX, XXX−XXX

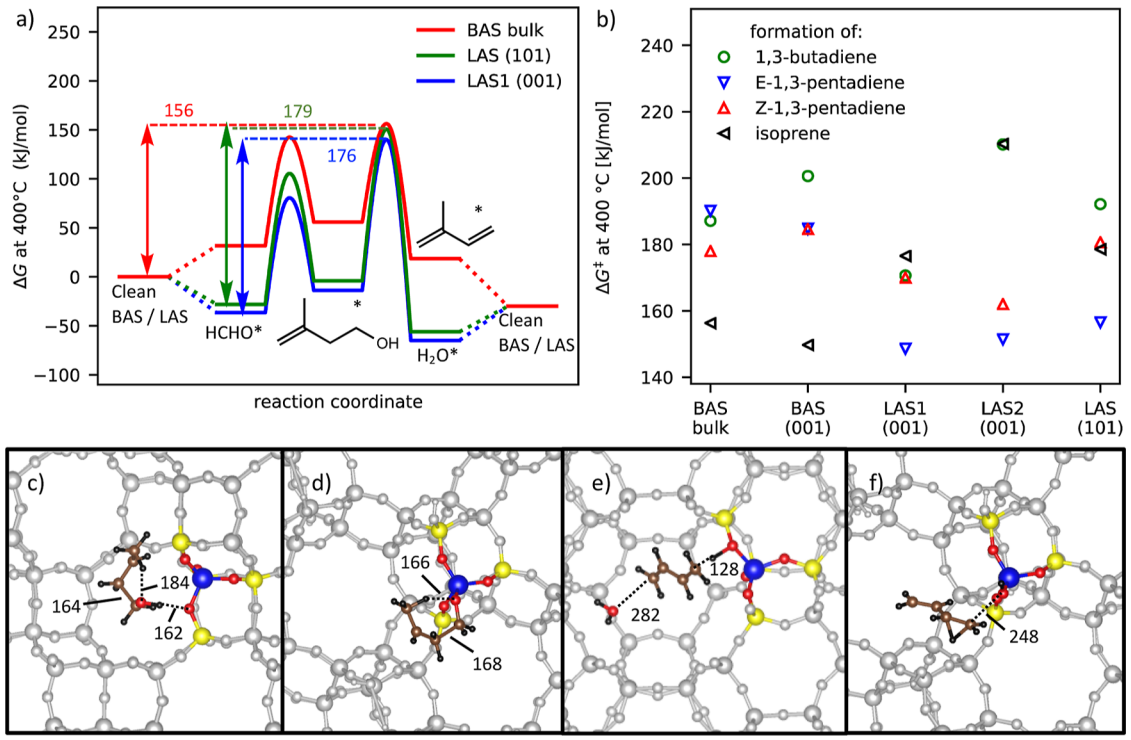

Figure 6. (a) Reaction free energy barriers of the Prins reaction at 400 °C and a reference pressure of 1 bar for each reactant. References state the clean acid site and molecules in the gas phase for BAS and HCHO adsorbed on the acid site with alkene in the gas phase for LAS. (b) Gibbs free energy diagram of the Prins reaction with isobutene at bulk BAS, LAS1(001), and LAS(101) at 400 °C and a reference pressure for each reactant of 1 bar. References are the clean acid site and molecules in the gas phase for BAS and HCHO adsorbed on the acid site with isobutene in the gas phase for LAS. (c–f) Transition state structures of the Prins reaction with propene at (c) bulk BAS and (d) LAS(101), butenol dehydration at (e) bulk BAS, and (f) LAS(101). Color code: blue: aluminum, yellow: silicon, red: oxygen, black: hydrogen, and brown: carbon.

Al and a proton at the adjacent oxygen. As we mentioned above, this arrangement is unstable with respect to the adsorption of a H_2O molecule,[44] which is formed immediately and with only a small barrier involved. Dehydration of 3-methyl-3-butenol proceeds via this E2-like mechanism for all three LAS, as well as dehydration of 3-butenol at LAS2(001). Nevertheless, differences between the reaction barriers of both pathways are moderate; the values for both mechanisms can be found in Table S8.

At BAS (Scheme 2b), isomerization of 3-butene-1-ol leads to an alcohol with a double bond in the β-position to the alcohol group (2-butene-1-ol in Scheme 2b). When the alcohol is protonated, the molecule can be arranged in such a way that H_2O leaves the molecule while the fourth carbon atom is concertedly deprotonated. As opposed to the mechanism for LAS, the final state is the diene adsorbed at the acid site and H_2O in the gas phase. The dehydration of the protonated alcohol is similar to the mechanism investigated by Kilburn et al.[75] where the authors investigated the coupling of HCHO with propene and further dehydration of butenol to butadiene at 433 K. They studied a different mechanism for the coupling of HCHO and propene to form 2-butene-1-ol directly, for which we found higher barriers than for the mechanism described above in our investigation. This is in agreement with Vasiliadou et al.,[76] who studied the Prins reaction for different butene isomers both experimentally and computationally, using a six-membered ring transition state to model the coupling of HCHO and olefin.

In all investigated reactions, the barrier of HCHO and olefin coupling is lower in Gibbs free energy than that in the following dehydration or isomerization steps. Figure 6b shows the reaction barriers for the overall reaction from HCHO and olefin to diene and H_2O, which is dehydration in the case of LAS and isomerization in most cases at BAS (see Supporting Information for details). At the surface BAS, reaction barriers for the formation of 1,3-butadiene and *Z*-1,3-pentadiene are higher by 13 and 6 kJ/mol than the respective barriers at bulk BAS, and they are lower by 6 and 7 kJ/mol for *E*-1,3-pentadiene and isoprene formation. At all LAS, the reaction barriers are lower for the formation of pentadienes than for the formation of butadiene and isoprene. When BAS and LAS are compared, the largest difference is seen in the formation of isoprene: this reaction has the lowest barriers of all investigated reactions at BAS and the highest barriers at LAS1(001) and LAS2(001). Barriers at LAS1(001) are on average 11 kJ/mol lower than the respective barriers at LAS(101), but this difference is not as pronounced as that for the HT reactions.

Figure 6a shows the Gibbs free energy diagram of isoprene formation at bulk BAS, LAS1(001), and LAS(101). Adsorption is stronger at the LAS, so different references are taken for the barrier heights (indicated by colored arrows in the figure). The last adsorption step is different for LAS and BAS: at LAS, H_2O is adsorbed, whereas BAS adsorbs isoprene. For bulk BAS and LAS(101), Figure 6c–f shows one example of the transition state structures for C–C bond formation and alcohol dehydration at LAS and BAS, respectively. The Prins reaction with several butene isomers on H-ZSM-5 has been experimentally (Prins coupling and alcohol dehydration) and computationally (only Prins coupling to the intermediate alcohol) studied by Vasiliadou et al.[76] They found that of the three investigated butene isomers (isobutene, 1-butene, and 2-butene), isobutene was the most reactive isomer. With an

https://doi.org/10.1021/acs.jpcc.4c03408
J. Phys. Chem. C XXXX, XXX, XXX−XXX

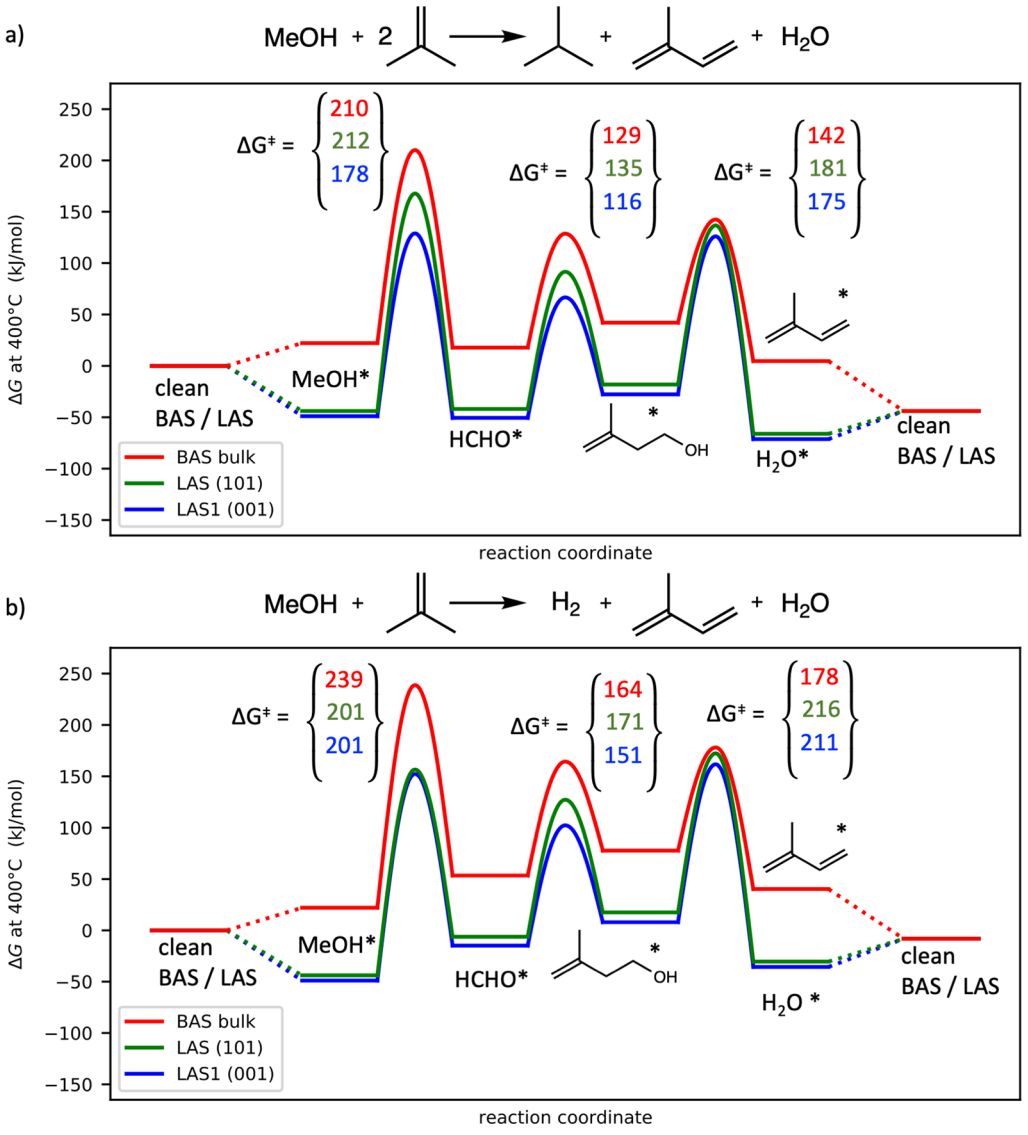

Figure 7. (a) Gibbs free energy diagram of the HT reaction with isobutene, followed by the Prins reaction of HCHO and isobutene to isoprene. (b) Gibbs free energy diagram of MeOH decomposition to HCHO, followed by the Prins reaction of HCHO and isobutene to isoprene. References are the clean acid site and MeOH in gas phase for BAS and MeOH adsorbed on the acid site for LAS. Reaction temperature is 400 °C and the reference pressure for all reactants is 1 bar.

ONIOM cluster model approach,[76] they calculated the reaction barriers of the Prins reaction from isobutene and 1-butene to 3-methyl-3-butenol and 3-*E*-pentenol to be 24 and 37 kJ/mol, respectively (H-ZSM-5, 150 °C), thus isobutene having a lower barrier by about 13 kJ/mol. In our calculations with H-SSZ-13 as the catalyst and thermal corrections for 150 °C, the reaction barrier of butene to 3-*E*-pentenol is 101 kJ/mol and that from isobutene to 3-methyl-3-butenol is 67 kJ/mol, so we find the same trend here.

Complete Reaction Mechanism. Finally, we analyze the full reaction mechanism to investigate the hypothesis, that HT from MeOH to alkenes takes place at LAS, but the Prins reaction and diene formation takes place at BAS.[28] We compared the reaction pathway of MeOH-mediated HT to isobutene, followed by the Prins reaction with a second isobutene (Scheme 1, reactions 1a and 2) with MeOH decomposition, followed by the same Prins reaction (Scheme 1, reactions 1b and 2). The corresponding Gibbs free energy diagrams are shown in Figure 7. When HCHO is produced by HT (Figure 7a), the transition state of the HT reaction is 31 kJ/mol higher in Gibbs free energy than the respective alcohol dehydration barrier (third barrier in Figure 7) for LAS(101), and 68 kJ/mol for BAS bulk. For LAS1(001), the dehydration barrier is lower than the HCHO formation barrier by 3 kJ/mol.

If HCHO is produced by MeOH decomposition (Figure 7b), the barrier of the alcohol dehydration is 15 and 10 kJ/mol higher than that of MeOH decomposition for LAS(101) and LAS1(001), while at BAS, MeOH decomposition has a 61 kJ/mol higher barrier than HCHO consumption. These combined pathways show that catalysts containing both BAS and LAS might have a higher activity. We note that diffusion of small molecules such as HCHO to overcome the distance between surface LAS and bulk BAS should proceed with rather small barriers.[77] Both reaction pathways differ only in the mechanism for formaldehyde formation but are identical in the Prins reactions, which couple formaldehyde with olefin. However, formaldehyde formation with the formation of either H_2 or an alkane as a byproduct differs in reaction free energy,

https://doi.org/10.1021/acs.jpcc.4c03408
J. Phys. Chem. C XXXX, XXX, XXX−XXX

where alkane formation is more favorable. This shifts the free energy of formaldehyde as the reference state and therefore also influences the Gibbs free energies of the transition states of the Prins reactions, given relative to the reactants. Since H_2-formation is less favorable thermodynamically, the Prins reactions appear less favorable in the Gibbs free energy diagram with transition states that are higher by 35 kJ/mol. However, it is important to point out that the Gibbs free energy diagram is given for a reference pressure of 1 bar for all species. Under MTO conditions, only a small part of MeOH is converted into HCHO,[29] which can rapidly undergo further reactions with olefins,[36] so the partial pressure of HCHO and H_2 is expected to be much lower than the pressure used in our calculations. This would make the reverse reaction of HCHO to methanol less likely than the Gibbs free energy diagram suggests. Overall, the kinetics of the Prins reaction will depend on the actual partial pressures, and this cannot be predicted for all possible situations just based on a Gibbs free energy diagram.

Scheme 3 shows the connections between MeOH, HCHO, and dienes. At the investigated reaction conditions, HT reaction barriers are similar for the two dominant acid sites [bulk BAS and LAS(101)], but the barrier at LAS1(001) is around 35 kJ/mol lower. Formaldehyde formation by methanol decomposition is 38 kJ/mol more favorable on LAS than on BAS, and the reverse reaction (formaldehyde hydrogenation) is also clearly more favorable on LAS than on BAS.

Scheme 3. Overview of the Reactions Investigated in This Work and Their Gibbs Free Energy Barriers at Bulk BAS, LAS1(001), and LAS(101) at 400 °C[a]

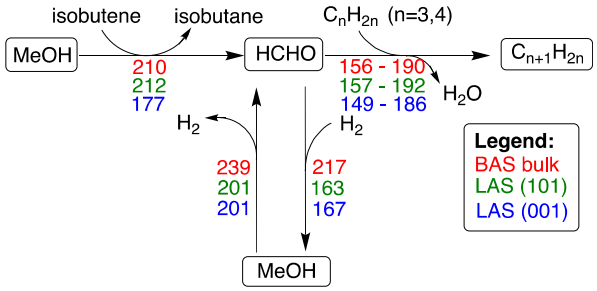

[a]Barriers at LAS are referenced to MeOH or HCHO adsorbed on the acid site, barriers at BAS are referenced to the clean acid site, and all reactants in the gas phase. For the Prins reaction, a range of barriers is given, corresponding to the different olefins studied, from propene to isobutene.

CONCLUSIONS

The formation of dienes from olefins and methanol was studied computationally for surface LAS and surface and bulk BAS of H-SSZ-13. Three different LAS were investigated, denoted LAS1(001), LAS2(001), and LAS(101), which occur on two different surfaces (001 and 101) of H-SSZ-13. The investigated mechanism for diene formation proceeds in two steps: (1) the formation of formaldehyde (HCHO) from methanol and (2) the coupling of HCHO with olefins (Prins reaction). Step (1) may proceed either via direct decomposition of methanol to H_2 and HCHO or via HT from MTO, resulting in the formation of HCHO and an alkane.

Generally, all involved molecules, both olefins and oxygenates, adsorb more strongly at LAS. Reaction barriers of the MeOH-mediated HT reactions are similar for two of the investigated LAS [LAS2(001) and LAS(101)] and both BAS, while LAS1(001) shows significantly lower reaction barriers (on average 30 kJ/mol compared to the other two LAS). For other reactions, barriers for the three investigated LAS are more similar. MeOH decomposition to HCHO and H_2 is clearly more favorable at LAS than at BAS, also for the backward reaction (hydrogenation of formaldehyde), which may be important for reactions cofeeding molecular hydrogen. Here, the barriers are at least 15 kJ/mol lower for the forward reaction and at least 50 kJ/mol lower for the backward reaction compared to BAS.

The Prins reaction involves two general steps: coupling of HCHO and the olefin, and dehydration of the formed alcohol to the diene. The activity of the investigated active sites depends on the substrate. For the formation of butadiene, *E*-pentadiene, and *Z*-pentadiene, we find that dehydration at LAS is more favorable by on average 13, 35, and 10 kJ/mol, not considering the extremely high value for butadiene formation at LAS2(001). Isoprene (2-methylbuta-1,3-diene), however, shows significantly lower diene formation barriers at BAS than at LAS (35 kJ/mol on average).

The barriers of the coupling of HCHO and olefin are on all sites lower than the respective dehydration barriers of the corresponding alcohols.

Besides the discussed barriers, the amount of dienes formed through the Prins reaction will depend on the concentration of the olefins and methanol.

In further investigations, not only surface LAS but also other LAS types, like EFAL, should be taken into account since they represent a large fraction of Lewis acidity in zeolites.

ASSOCIATED CONTENT

Supporting Information

The Supporting Information is available free of charge at https://pubs.acs.org/doi/10.1021/acs.jpcc.4c03408.

Additional analysis, Bader charges, and total energies (PDF)

Coordinates of the investigated structures (TXT)

AUTHOR INFORMATION

Corresponding Authors

Philipp N. Plessow − *Institute of Catalysis Research and Technology, Karlsruhe Institute of Technology, 76344 Eggenstein-Leopoldshafen, Germany;* orcid.org/0000-0001-9913-4049; Email: philipp.plessow@kit.edu

Felix Studt − *Institute of Catalysis Research and Technology, Karlsruhe Institute of Technology, 76344 Eggenstein-Leopoldshafen, Germany; Institute for Chemical Technology and Polymer Chemistry, Karlsruhe Institute of Technology, 76131 Karlsruhe, Germany;* orcid.org/0000-0001-6841-4232; Email: felix.studt@kit.edu

Authors

Annika E. Enss − *Institute of Catalysis Research and Technology, Karlsruhe Institute of Technology, 76344 Eggenstein-Leopoldshafen, Germany*

Philipp Huber − *Institute of Catalysis Research and Technology, Karlsruhe Institute of Technology, 76344 Eggenstein-Leopoldshafen, Germany*

https://doi.org/10.1021/acs.jpcc.4c03408
J. Phys. Chem. C XXXX, XXX, XXX−XXX

Complete contact information is available at:
https://pubs.acs.org/10.1021/acs.jpcc.4c03408

Notes

The authors declare no competing financial interest.
Published as part of *The Journal of Physical Chemistry C* special issue "Jens K. Nørskov Festschrift".

■ ACKNOWLEDGMENTS

The authors acknowledge support by the state of Baden-Württemberg through bwHPC and the German Research Foundation (DFG) through grant no INST 40/575-1 FUGG (JUSTUS 2 cluster) and bwunicluster.

■ REFERENCES

(1) Olsbye, U.; Svelle, S.; Bjørgen, M.; Beato, P.; Janssens, T. V. W.; Joensen, F.; Bor-diga, S.; Lillerud, K. P. Conversion of Methanol to Hydrocarbons: How Zeolite Cavity and Pore Size Controls Product Selectivity. *Angew. Chem., Int. Ed.* **2012**, *51*, 5810−5831.
(2) Olah, G. A. Beyond Oil and Gas: The Methanol Economy. *Angew. Chem., Int. Ed.* **2005**, *44*, 2636−2639.
(3) Olah, G. A. Towards Oil Independence Through Renewable Methanol Chemistry. *Angew. Chem., Int. Ed.* **2013**, *52*, 104−107.
(4) Hemelsoet, K.; Van der Mynsbrugge, J.; De Wispelaere, K.; Waroquier, M.; Van Spey-broeck, V. Unraveling the Reaction Mechanisms Governing Methanol-to-Olefins Catal- ysis by Theory and Experiment. *ChemPhysChem* **2013**, *14*, 1526−1545.
(5) Yarulina, I.; Chowdhury, A. D.; Meirer, F.; Weckhuysen, B. M.; Gascon, J. Recent trends and fundamental insights in the methanol-to-hydrocarbons process. *Nat. Catal.* **2018**, *1*, 398−411.
(6) Ilias, S.; Bhan, A. Mechanism of the Catalytic Conversion of Methanol to Hydrocarbons. *ACS Catal.* **2013**, *3*, 18−31.
(7) Dahl, I. M.; Kolboe, S. On the reaction mechanism for propene formation in the MTO reaction over SAPO-34. *Catal. Lett.* **1993**, *20*, 329−336.
(8) Dahl, I.; Kolboe, S. On the Reaction Mechanism for Hydrocarbon Formation from Methanol over SAPO-34. *J. Catal.* **1994**, *149*, 458−464.
(9) Dahl, I. M.; Kolboe, S. On the Reaction Mechanism for Hydrocarbon Formation from Methanol over SAPO-34. *J. Catal.* **1996**, *161*, 304−309.
(10) Bleken, F.; Bjørgen, M.; Palumbo, L.; Bordiga, S.; Svelle, S.; Lillerud, K.-P.; Olsbye, U. The Effect of Acid Strength on the Conversion of Methanol to Olefins Over Acidic Microporous Catalysts with the CHA Topology. *Top. Catal.* **2009**, *52*, 218−228.
(11) Zapater, D.; Lasobras, J.; Soler, J.; Herguido, J.; Menéndez, M. MTO with SAPO-34 in a Fixed-Bed Reactor: Deactivation Profiles. *Ind. Eng. Chem. Res.* **2021**, *60*, 16162−16170.
(12) Gao, M.; Li, H.; Yang, M.; Zhou, J.; Yuan, X.; Tian, P.; Ye, M.; Liu, Z. A modeling study on reaction and diffusion in MTO process over SAPO-34 zeolites. *Chem. Eng. J.* **2019**, *377*, 119668.
(13) Zhou, J.; Gao, M.; Zhang, J.; Liu, W.; Zhang, T.; Li, H.; Xu, Z.; Ye, M.; Liu, Z. Directed transforming of coke to active intermediates in methanol-to-olefins catalyst to boost light olefins selectivity. *Nat. Commun.* **2021**, *12*, 17.
(14) Fu, H.; Song, W.; Haw, J. F. Polycyclic Aromatics Formation in HSAPO-34 Dur- ing Methanol-to-Olefin Catalysis: Ex Situ Characterization After Cryogenic Grinding. *Catal. Lett.* **2001**, *76*, 89−94.
(15) Wragg, D. S.; O'Brien, M. G.; Bleken, F. L.; Di Michiel, M.; Olsbye, U.; Fjellvåg, H. Watching the Methanol-to-Olefin Process with Time- and Space-Resolved High-Energy Operando X-ray Diffraction. *Angew. Chem., Int. Ed.* **2012**, *51*, 7956−7959.
(16) Hwang, A.; Bhan, A. Deactivation of Zeolites and Zeotypes in Methanol-to- Hydrocarbons Catalysis: Mechanisms and Circumvention. *Acc. Chem. Res.* **2019**, *52*, 2647−2656.
(17) Rojo-Gama, D.; Signorile, M.; Bonino, F.; Bordiga, S.; Olsbye, U.; Lillerud, K. P.; Beato, P.; Svelle, S. Structure-deactivation relationships in zeolites during the methanol-to-hydrocarbons reaction: Complementary assessments of the coke content. *J. Catal.* **2017**, *351*, 33−48.
(18) Bleken, F. L.; Barbera, K.; Bonino, F.; Olsbye, U.; Lillerud, K. P.; Bordiga, S.; Beato, P.; Janssens, T. V.; Svelle, S. Catalyst deactivation by coke formation in micro- porous and desilicated zeolite H-ZSM-5 during the conversion of methanol to hydrocarbons. *J. Catal.* **2013**, *307*, 62−73.
(19) Montalvo-Castro, H.; DeLuca, M.; Kilburn, L.; Hibbitts, D. Mechanisms and Kinetics of the Dehydrogenation of C_6-C_8 Cycloalkanes, Cycloalkenes, and Cyclodienes to Aromatics in H-MFI Zeolite Framework. *ACS Catal.* **2023**, *13*, 99−112.
(20) Foley, B. L.; Bhan, A. Transient and Steady-State Kinetic Studies of Formaldehyde Alkylation of Benzene to Form Diphenylmethane on HZSM-5 Catalysts. *ACS Catal.* **2020**, *10*, 10436−10448.
(21) Foley, B. L.; Johnson, B. A.; Bhan, A. Kinetic Evaluation of Deactivation Pathways in Methanol-to-Hydrocarbon Catalysis on HZSM-5 with Formaldehyde, Olefinic, Dieneic, and Aromatic Co-Feeds. *ACS Catal.* **2021**, *11*, 3628−3637.
(22) Martinez-Espin, J. S.; Mortén, M.; Janssens, T. V. W.; Svelle, S.; Beato, P.; Ols-bye, U. New insights into catalyst deactivation and product distribution of zeolites in the methanol-to-hydrocarbons (MTH) reaction with methanol and dimethyl ether feeds. *Catal. Sci. Technol.* **2017**, *7*, 2700−2716.
(23) Bollini, P.; Chen, T. T.; Neurock, M.; Bhan, A. Mechanistic role of water in HSSZ-13 catalyzed methanol-to-olefins conversion. *Catal. Sci. Technol.* **2019**, *9*, 4374−4383.
(24) Arora, S. S.; Nieskens, D. L. S.; Malek, A.; Bhan, A. Lifetime improvement in methanol- to-olefins catalysis over chabazite materials by high-pressure H2 co-feeds. *Nat. Catal.* **2018**, *1*, 666−672.
(25) Arora, S. S.; Shi, Z.; Bhan, A. Mechanistic Basis for Effects of High-Pressure H_2 Cofeeds on Methanol-to-Hydrocarbons Catalysis over Zeolites. *ACS Catal.* **2019**, *9*, 6407−6414.
(26) DeLuca, M.; Janes, C.; Hibbitts, D. Contrasting Arene, Alkene, Diene, and Formalde- hyde Hydrogenation in H-ZSM-5, H-SSZ-13, and H-SAPO-34 Frameworks during MTO. *ACS Catal.* **2020**, *10*, 4593−4607.
(27) Xie, J.; Firth, D. S.; Cordero-Lanzac, T.; Airi, A.; Negri, C.; Øien-Ødegaard, S.; Lillerud, K. P.; Bordiga, S.; Olsbye, U. MAPO-18 Catalysts for the Methanol to Olefins Process: Influence of Catalyst Acidity in a High-Pressure Syngas (CO and H_2) Envi- ronment. *ACS Catal.* **2022**, *12*, 1520−1531.
(28) Müller, S.; Liu, Y.; Kirchberger, F. M.; Tonigold, M.; Sanchez-Sanchez, M.; Lercher, J. A. Hydrogen Transfer Pathways during Zeolite Catalyzed Methanol Con- version to Hydrocarbons. *J. Am. Chem. Soc.* **2016**, *138*, 15994−16003.
(29) Liu, Y.; Kirchberger, F. M.; Müller, S.; Eder, M.; Tonigold, M.; Sanchez-Sanchez, M.; Lercher, J. A. Critical role of formaldehyde during methanol conversion to hydrocar- bons. *Nat. Commun.* **2019**, *10*, 1462.
(30) Krieger, A. M.; Sinha, V.; Li, G.; Pidko, E. A. Solvent-Assisted Ketone Reduction by a Homogeneous Mn Catalyst. *Organometallics* **2022**, *41*, 1829−1835.
(31) Carr, C. R.; Vesto, J. I.; Xing, X.; Fettinger, J. C.; Berben, L. A. Aluminum-Ligand Cooperative OH Bond Activation Initiates Catalytic Transfer Hydrogenation. *ChemCatChem* **2022**, *14*, No. e202101869.
(32) Liu, Y.; Müller, S.; Berger, D.; Jelic, J.; Reuter, K.; Tonigold, M.; Sanchez-Sanchez, M.; Lercher, J. A. Formation Mechanism of the First Carbon-Carbon Bond and the First Olefin in the Methanol Conversion into Hydrocarbons. *Angew. Chem., Int. Ed.* **2016**, *55*, 5723−5726.
(33) Paunović, V.; Hemberger, P.; Bodi, A.; Hauert, R.; Van Bokhoven, J. A. Impact of Nonzeolite-Catalyzed Formation of Formaldehyde on the Methanol-to-Hydrocarbons Conversion. *ACS Catal.* **2022**, *12*, 13426−13434.
(34) Comas-Vives, A.; Valla, M.; Copéret, C.; Sautet, P. Cooperativity between Al Sites Pro- motes Hydrogen Transfer and

Carbon-Carbon Bond Formation upon Dimethyl Ether Activation on Alumina. *ACS Cent. Sci.* **2015**, *1*, 313−319.
(35) Sun, X.; Mueller, S.; Liu, Y.; Shi, H.; Haller, G. L.; Sanchez-Sanchez, M.; van Veen, A. C.; Lercher, J. A. On reaction pathways in the conversion of methanol to hydrocarbons on HZSM-5. *J. Catal.* **2014**, *317*, 185−197.
(36) Wen, W.; Yu, S.; Zhou, C.; Ma, H.; Zhou, Z.; Cao, C.; Yang, J.; Xu, M.; Qi, F.; Zhang, G.; et al. Formation and Fate of Formaldehyde in Methanol-to-Hydrocarbon Reaction: In Situ Synchrotron Radiation Photoionization Mass Spectrometry Study. *Angew. Chem., Int. Ed.* **2020**, *59*, 4873−4878.
(37) Chen, K.; Gan, Z.; Horstmeier, S.; White, J. L. Distribution of Aluminum Species in Zeolite Catalysts: ^{27}Al NMR of Framework, Partially-Coordinated Framework, and Non-Framework Moieties. *J. Am. Chem. Soc.* **2021**, *143*, 6669−6680.
(38) Ravi, M.; Sushkevich, V. L.; van Bokhoven, J. A. Towards a better understanding of Lewis acidic aluminium in zeolites. *Nat. Mater.* **2020**, *19*, 1047−1056.
(39) Khramenkova, E. V.; Venkatraman, H.; Soethout, V.; Pidko, E. A. Global optimiza- tion of extraframework ensembles in zeolites: structural analysis of extraframework aluminum species in MOR and MFI zeolites. *Phys. Chem. Chem. Phys.* **2022**, *24*, 27047−27054.
(40) Jin, M.; Ravi, M.; Lei, C.; Heard, C. J.; Brivio, F.; Tošner, Z.; Grajciar, L.; Van Bokhoven, J. A.; Nachtigall, P. Dynamical Equilibrium between Brønsted and Lewis Sites in Zeolites: Framework-Associated Octahedral Aluminum. *Angew. Chem., Int. Ed.* **2023**, *62*, No. e202306183.
(41) Yakimov, A. V.; Ravi, M.; Verel, R.; Sushkevich, V. L.; Van Bokhoven, J. A.; Copéret, C. Structure and Framework Association of Lewis Acid Sites in MOR Ze- olite. *J. Am. Chem. Soc.* **2022**, *144*, 10377−10385.
(42) Treps, L.; Gomez, A.; de Bruin, T.; Chizallet, C. Environment, Stability and Acidity of External Surface Sites of Silicalite-1 and ZSM-5 Micro and Nano Slabs, Sheets, and Crystals. *ACS Catal.* **2020**, *10*, 3297−3312.
(43) Jarrin, T.; de Bruin, T.; Chizallet, C. Stability and acidity of sites at the external surface and at point defects of faujasite. *ChemCatChem* **2023**, *15*, No. e202201302.
(44) Huber, P.; Studt, F.; Plessow, P. N. Reactivity of Surface Lewis and Brønsted Acid Sites in Zeolite Catalysis: A Computational Case Study of DME Synthesis Using H-SSZ-13. *J. Phys. Chem. C* **2022**, *126*, 5896−5905.
(45) Balcom, H.; Hoffman, A. J.; Locht, H.; Hibbitts, D. Brønsted Acid Strength Does Not Change for Bulk and External Sites of MFI Except for Al Substitution Where Silanol Groups Form. *ACS Catal.* **2023**, *13*, 4470−4487.
(46) Perdew, J. P.; Burke, K.; Ernzerhof, M. Generalized Gradient Approximation Made Simple. *Phys. Rev. Lett.* **1996**, *77*, 3865−3868.
(47) Grimme, S.; Antony, J.; Ehrlich, S.; Krieg, H. A consistent and accurate *ab initio* parametrization of density functional dispersion correction (DFT-D) for the 94 elements H-Pu. *J. Chem. Phys.* **2010**, *132*, 154104.
(48) Kresse, G.; Joubert, D. From ultrasoft pseudopotentials to the projector augmented- wave method. *Phys. Rev. B: Condens. Matter Mater. Phys.* **1999**, *59*, 1758−1775.
(49) Hjorth Larsen, A.; Jorgen Mortensen, J.; Blomqvist, J.; Castelli, I. E.; Christensen, R.; Dulak, M.; Friis, J.; Groves, M. N.; Hammer, B.; Hargus, C.; et al. The atomic simulation environment—a Python library for working with atoms. *J. Phys.: Condens. Matter* **2017**, *29*, 273002.
(50) Brogaard, R. Y.; Henry, R.; Schuurman, Y.; Medford, A. J.; Moses, P. G.; Beato, P.; Svelle, S.; Nørskov, J. K.; Olsbye, U. Methanol-to-hydrocarbons conversion: The alkene methylation pathway. *J. Catal.* **2014**, *314*, 159−169.
(51) Brogaard, R. Y.; Wang, C.-M.; Studt, F. Methanol-Alkene Reactions in Zeotype Acid Catalysts: Insights from a Descriptor-Based Approach and Microkinetic Modeling. *ACS Catal.* **2014**, *4*, 4504−4509.
(52) Plessow, P. N. Efficient Transition State Optimization of Periodic Structures through Automated Relaxed Potential Energy Surface Scans. *J. Chem. Theory Comput.* **2018**, *14*, 981−990.
(53) Rybicki, M.; Sauer, J. Ab Initio Prediction of Proton Exchange Barriers for Alkanes at Brønsted Sites of Zeolite H-MFI. *J. Am. Chem. Soc.* **2018**, *140*, 18151−18161.
(54) Svelle, S.; Tuma, C.; Rozanska, X.; Kerber, T.; Sauer, J. Quantum Chemical Modeling of Zeolite-Catalyzed Methylation Reactions: Toward Chemical Accuracy for Barriers. *J. Am. Chem. Soc.* **2009**, *131*, 816−825.
(55) Hansen, N.; Kerber, T.; Sauer, J.; Bell, A. T.; Keil, F. J. Quantum Chemical Model- ing of Benzene Ethylation over H-ZSM-5 Approaching Chemical Accuracy: A Hybrid MP2:DFT Study. *J. Am. Chem. Soc.* **2010**, *132*, 11525−11538.
(56) Sauer, J. The future of computational catalysis. *J. Catal.* **2024**, *433*, 115482.
(57) Goncalves, T. J.; Plessow, P. N.; Studt, F. On the Accuracy of Density Functional Theory in Zeolite Catalysis. *ChemCatChem* **2019**, *11*, 4368−4376.
(58) Feller, D. Application of systematic sequences of wave functions to the water dimer. *J. Chem. Phys.* **1992**, *96*, 6104−6114.
(59) Helgaker, T.; Klopper, W.; Koch, H.; Noga, J. Basis-set convergence of correlated calculations on water. *J. Chem. Phys.* **1997**, *106*, 9639−9646.
(60) Neese, F. The ORCA program system. *Wiley Interdiscip. Rev.: Comput. Mol. Sci.* **2012**, *2*, 73−78.
(61) Dunning, T. H. Gaussian basis sets for use in correlated molecular calculations. I. The atoms boron through neon and hydrogen. *J. Chem. Phys.* **1989**, *90*, 1007−1023.
(62) Minenkov, Y.; Bistoni, G.; Riplinger, C.; Auer, A. A.; Neese, F.; Cavallo, L. Pair natural orbital and canonical coupled cluster reaction enthalpies involving light to heavy alkali and alkaline earth metals: the importance of sub-valence correlation. *Phys. Chem. Chem. Phys.* **2017**, *19*, 9374−9391.
(63) Riplinger, C.; Pinski, P.; Becker, U.; Valeev, E. F.; Neese, F. Sparse maps—A system- atic infrastructure for reduced-scaling electronic structure methods. II. Linear scaling domain based pair natural orbital coupled cluster theory. *J. Chem. Phys.* **2016**, *144*, 024109.
(64) Saitow, M.; Becker, U.; Riplinger, C.; Valeev, E. F.; Neese, F. A new near-linear scaling, efficient and accurate, open-shell domain-based local pair natural orbital coupled cluster singles and doubles theory. *J. Chem. Phys.* **2017**, *146*, 164105.
(65) Neese, F.; Wennmohs, F.; Hansen, A.; Becker, U. Efficient, approximate and paral- lel Hartree-Fock and hybrid DFT calculations. A 'chain-of-spheres' algorithm for the Hartree-Fock exchange. *Chem. Phys.* **2009**, *356*, 98−109.
(66) Ahlrichs, R.; Bär, M.; Häser, M.; Horn, H.; Kölmel, C. Electronic structure calculations on workstation computers: The program system turbomole. *Chem. Phys. Lett.* **1989**, *162*, 165−169.
(67) Weigend, F.; Ahlrichs, R. Balanced basis sets of split valence, triple zeta valence and quadruple zeta valence quality for H to Rn: Design and assessment of accuracy. *Phys. Chem. Chem. Phys.* **2005**, *7*, 3297.
(68) Weigend, F.; Furche, F.; Ahlrichs, R. Gaussian basis sets of quadruple zeta valence quality for atoms H-Kr. *J. Chem. Phys.* **2003**, *119*, 12753−12762.
(69) Eichkorn, K.; Treutler, O.; Öhm, H.; Häser, M.; Ahlrichs, R. Auxiliary basis sets to approximate Coulomb potentials. *Chem. Phys. Lett.* **1995**, *240*, 283−290.
(70) Plessow, P. N.; Studt, F. Unraveling the Mechanism of the Initiation Reaction of the Methanol to Olefins Process Using ab Initio and DFT Calculations. *ACS Catal.* **2017**, *7*, 7987−7994.
(71) Nguyen, H. G.; Konya, G.; Eyring, E. M.; Hunter, D. B.; Truong, T. N. Theoretical Study on the Interaction between Xenon and Positively Charged Silver Clusters in Gas Phase and on the (001) Chabazite Surface. *J. Phys. Chem. C* **2009**, *113*, 12818−12825.
(72) Kozuch, S.; Shaik, S. How to Conceptualize Catalytic Cycles? The Energetic Span Model. *Acc. Chem. Res.* **2011**, *44*, 101−110.

https://doi.org/10.1021/acs.jpcc.4c03408
J. Phys. Chem. C XXXX, XXX, XXX−XXX

(73) Larmier, K.; Chizallet, C.; Cadran, N.; Maury, S.; Abboud, J.; Lamic-Humblot, A.-F.; Marceau, E.; Lauron-Pernot, H. Mechanistic Investigation of Isopropanol Conversion on Alumina Catalysts: Location of Active Sites for Alkene/Ether Production. *ACS Catal.* **2015**, *5*, 4423−4437.
(74) Larmier, K.; Chizallet, C.; Maury, S.; Cadran, N.; Abboud, J.; Lamic-Humblot, A.; Marceau, E.; Lauron-Pernot, H. Isopropanol Dehydration on Amorphous Sil- ica-Alumina: Synergy of Brønsted and Lewis Acidities at Pseudo-Bridging Silanols. *Angew. Chem., Int. Ed.* **2017**, *56*, 230−234.
(75) Kilburn, L.; DeLuca, M.; Hoffman, A. J.; Patel, S.; Hibbitts, D. Comparing alkene-mediated and formaldehyde-mediated diene formation routes in methanol-to-olefins catalysis in MFI and CHA. *J. Catal.* **2021**, *400*, 124−139.
(76) Vasiliadou, E. S.; Li, S.; Caratzoulas, S.; Lobo, R. F. Formaldehyde-isobutene Prins condensation over MFI-type zeolites. *Catal. Sci. Technol.* **2018**, *8*, 5794−5806.
(77) Smith, A. T.; Plessow, P. N.; Studt, F. Density functional theory calculations of diffu- sion barriers of organic molecules through the 8-ring of H-SSZ-13. *Chem. Phys.* **2021**, *541*, 111033.

https://doi.org/10.1021/acs.jpcc.4c03408
J. Phys. Chem. C XXXX, XXX, XXX−XXX